ChemComm

Accepted Manuscript

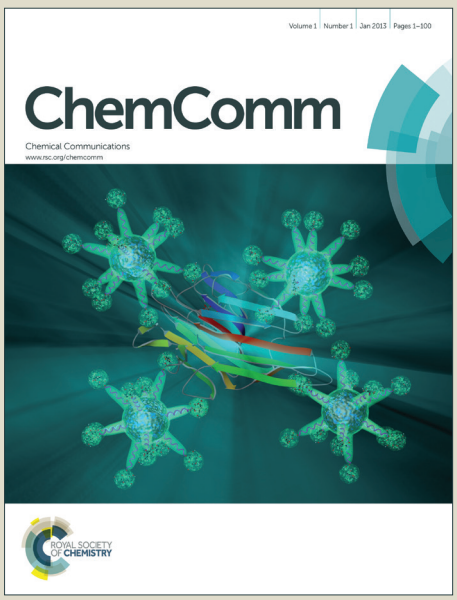

ROYAL SOCIETY OF CHEMISTRY

www.rsc.org/chemcomm

Journal Name

Dynamic Article Links ►

Cite this: DOI: 10.1039/c0xx00000x

www.rsc.org/xxxxxx

ARTICLE TYPE

Reversible Sodium Storage via Conversion Reaction in MoS_2/C Composite

Yun-Xiao Wang,[a] Kuok Hau Seng,[a] Shu-Lei Chou,*[a] Jiazhao Wang,[a] Zaiping Guo,[a] David Wexler,[a] Hua-Kun Liu,[a] Shi-Xue Dou[a]

Received (in XXX, XXX) Xth XXXXXXXXX 20XX, Accepted Xth XXXXXXXXX 20XX
DOI: 10.1039/b000000x

An exfoliated MoS_2/C composite (E-MoS_2/C) was prepared via simple chemical exfoliation and hydrothermal method. The obtained E-MoS_2/C was tested as a anode material for the sodium ion battery. High capacity (~400 mAh g^{-1}) at 0.25 C (100 mA g^{-1}) is maintained over prolonged cycling life (100 cycles). Outstanding rate capability is also achieved with a capacity of 290 mAh g^{-1} at 5 C.

Lithium-ion batteries (LIBs) have been widely used as the power sources for the small electronic devices in our daily lives due to their high energy densities.[1,2] However, LIBs are confronting a huge challenge to satisfy the demands of the ever growing electronic and electric vehicle markets. Plenty of reseraches turn to new battery systems, including aqueous batteries,[3,4] and hybrid batteries.[5] Rechargeable sodium ion batteries (SIBs) are especially regaining interest for use in large-scale applications because of their huge advantages in terms of low cost and the abundance of sodium resources. The ionic radius of sodium (0.102 nm) is larger compared to lithium (0.076 nm), and successfully reversible electrode materials are required to possess large enough channels and/or interstitial sites.[6] Molybdenum disulphide (MoS_2) has been extensively investigated for a long time due to its great potential for applications in the field of hydrogen storage,[7] medical and optoelectronics,[8] magnesium ion batteries,[9,10] and lithium ion batteries.[11-13] As a typical layered transition metal chalcogenide, MoS_2 has a graphite-like structure, where Mo and S atoms are covalently bonded to form two-dimensional S-Mo-S trilayers. These layers are then stacked together through weak van der Waals forces between the S^{2-} layers, forming a sandwich structure. It is not surprising, therefore, that MoS_2 could be a desirable intercalation host material because the guest atoms could reversibly intercalate into the weakly bound stacked layers. Recently, Park et. al reported the possibility of commercial MoS_2 for sodium-ion storage[14]. However, the MoS_2 only deliver a very low capacity of 85 mAh g^{-1} during 0.4 to 2.6 V by intercalation/deintercalation reaction. Based on our recent work, pristine MoS_2 is proven to conduct reversible conversion reaction (~3 Na^+ reaction, ~501 mAh g^{-1}) by further discharged to lower voltage (0.01 V).[15] Therefore, there is significant room to enhance the reversible capacity of MoS_2 via the realization of conversion reaction.

Herein, we report on an exfoliated MoS_2/C composite (E-MoS_2/C) for SIBs with outstanding electrochemical properties. As shown in Fig. 1a, the synthesis processes consist of two steps, including chemical exfoliation and hydrothermal method (details in supporting information). Our strategy to achieve high performances is to use a unique E-MoS_2/C as an anode material that possesses expanded *d*-spacing to accommodate large sodium ions. The exfoliated structure could shorten the Na-ion diffusion pathway and also withstand large volume change due to the buffering space created by the crumpled nanosheets. Simultaneously, the carbon component can effectively increase electrode

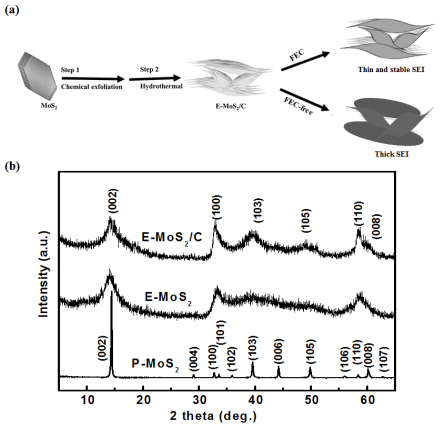

Fig. 1 (a) Schematic illustration of preparation of E-MoS_2/C and the effect of FEC additive, and (b) XRD patterns of P-MoS_2, E-MoS_2, and E-MoS_2/C

Journal Name

Dynamic Article Links ►

Cite this: DOI: 10.1039/c0xx00000x

www.rsc.org/xxxxxx

ARTICLE TYPE

conductivity. On the other hand, various electrolytes were utilized to optimize the cycling performance of E-MoS_2/C. The E-MoS_2/C is presented as an excellent anode material in 1.0 M $NaClO_4$ with propylene carbonate / ethylene carbonate and 5 wt % fluoroethylene carbonate additive (PC/EC + 5 wt % FEC), which is tend to form thin and stable SEI film due to the FEC reaction with electrolyte.

The X-ray diffraction (XRD) patterns of pristine MoS_2 (P-MoS_2), exfoliated MoS_2 (E-MoS_2), and E-MoS_2/C are presented in Fig. 1b, all of which can be indexed to the hexagonal 2H-MoS_2 structure (JPCDS No. 37–1492). P-MoS_2 shows more sharp peaks with higher intensity, indicating its good crystallinity with good ordering and well-stacked layered structure. In contrast, E-MoS_2 and E-MoS_2/C show broadened peaks with weakened (002) diffraction peaks, demonstrating smaller crystallite size and a decrease in the number of stacking layers. Furthermore, as shown in Fig. S1a the 2 θ value of the (002) diffraction peak has shifted to a lower angle of 13.98° and 14.02° for E-MoS_2 and E-MoS_2/C, respectively. This corresponds to the increase in the interlayer distance of the (002) plane, which is 0.633 and 0.631 nm, respectively, according to the Bragg equation. Moreover, no characteristic peak of carbon can be detected in E-MoS_2/C, indicating the amorphous nature of the carbon. The carbon content is estimated to be approximately 9 wt % in the E-MoS_2/C by thermogravimetric analysis (TGA), as shown in Fig. S1b.

High resolution transmission electron microscope (HRTEM) images provided insight into the morphology and structure of the P-MoS_2, E-MoS_2, and E-MoS_2/C. The good crystallization and well-stacked layered structure of P-MoS_2 is verified as shown in Fig. 2a, with a interplanar distance of 0.61 nm. In contrast, E-MoS_2 and E-MoS_2/C (Fig. 2b, c and d) displays a relatively loose packing of nanosheets and presents a somewhat transparent appearance. It is also can be seen that the E-MoS_2/C possesses much smaller crystal size than P-MoS_2 and E-MoS_2 (Fig. S2f and g). Lattice fringes could be observed clearly, measured d-spacings of 0.63−0.65 nm and 0.62−0.64 nm for E-MoS_2 and E-MoS_2/C, respectively, which is consistent with XRD results. The number of restacked layers is less than 10 for E-MoS_2/C, which implies that the incorporation of carbon could restrain restacking of the MoS_2 layers. It is believed that the larger d-spacing and the smaller crystallite size are favourable to electrochemical storage of the larger sodium. The same conclusion could be drawn from the field emission scanning electron microscope (FESEM) in Fig. S2, It is clear that nanosheets of E-MoS_2/C are thinner than those of E-MoS_2. Energy dispersive X-ray (EDX) analysis at different points (Fig. S3) reveals that the E-MoS_2/C is composed of molybdenum, sulfur, and carbon, and confirms the homogenous dispersion of carbon in the E-MoS_2/C.

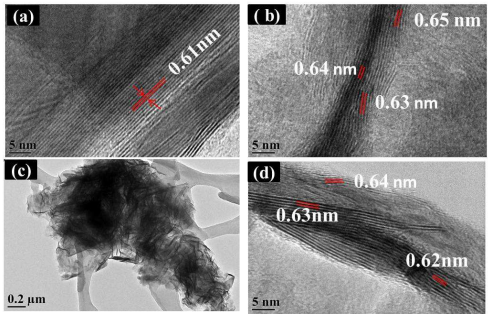

Fig. 2 HRTEM images of (a) P-MoS_2 and (b) E-MoS_2; TEM (c) and HRTEM (d) images E-MoS_2/C.

The electrochemical sodium-storage behaviours of these materials were investigated using galvanostatic discharge and cyclic voltammetry measurements using various electrolytes. As shown in Fig. S4, these electrodes show similar charge/discharge profiles, with slight variation in the plateau position. The shapes of the charge/discharge profiles are very similar to the report,[11] indicating a similar electrochemical storage mechanism. Three plateaus are observed in Fig. 3a at ~0.9 V, 0.73 V, and 0.1 V during the initial discharge process. The first strongly pronounced plateau at 0.9 V should be indicative of the formation of Na_xMoS_2, the plateau at 0.73 V is related to further Na ion reaction with MoS_2, and the long 0.1 V plateau should be related to the reduction of Mo^{4+} to Mo metal, accompanied by the formation of Na_2S nanoparticles. In the subsequent discharge process, the discharge profiles turn into sloping curves instead of those three plateaus, which indicates the occurence of the conversion reaction. During the initial charge process, a plateau at 1.85 V can be seen and is reversible in the following charge cycles, which is supposed to correspond to the redox reaction. There is a corresponding charge plateau at 2.2 V in LIBs.[11-13,16] The difference of ~0.3 V is attributed to the standard electrode potential difference (E^0_{Li/Li^+} - $E^0_{Na/Na+}$ = -0.33 V). It implies that there is a similar reaction mechanism of MoS_2 with both lithium and sodium. In brief, the charge/discharge curves of Na-MoS_2 show a sloping profile and voltage hysteresis, which resembles the Li-MoS_2 conversion

Journal Name

Dynamic Article Links ►

Cite this: DOI: 10.1039/c0xx00000x

www.rsc.org/xxxxxx

ARTICLE TYPE

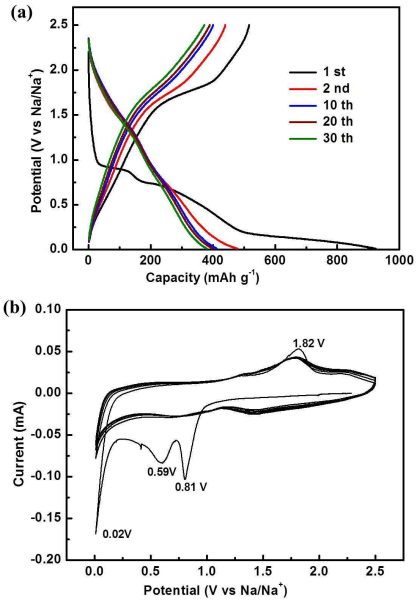

Fig. 3 (a) Charge/discharge profiles at 100 mA g^{-1}; (b) Cyclic voltammograms at a scan rate of 0.1 mV s^{-1} of E-MoS_2/C in in 1.0 M $NaClO_4$ with PC.

reaction. [11-13,16] The reaction mechanism of Na and E-MoS_2/C was further investigated by ex-situ XRD (Fig. S5) and XPS (Fig. S6). The electrode material showed the amorphous nature when the electrode was both fully discharged to 0.01 V and fully charge back to 2.5 V (Fig. S5). When the electrode was charged to 0.01 V, the Mo $3d_{5/2}$ peak (Fig. S6a) shifts to 227.5 eV, indicating the reduction of Mo^{4+} to Mo. A peak at 1071.2 eV (Fig. S6f) and a peak at 161.5 eV (Fig. S6e) can be indexed to the Na 1s and S $2p_{3/2}$ in Na_2S. When the electrode was charged to 2.5 V, the Mo $3d_{5/2}$ peak (Fig. S6g) appears at higher binding energy (~230.4 eV), and the S 1s energy binding is ~162.1 eV (Fig. S6h), indicating the recovery of MoS_2. The Na 1s peak at ca. 1071.5 eV (Fig. S6k) is probably ascribed to Na_2CO_3 in solid electrolyte interphase (SEI) film. It is noticeable that the intensity of Mo $3d_{5/2}$ and S 1s for MoS_2 is severely lowered, which is likely due to the formation of thick SEI film on electrode surface. Combining the ex-situ XRD and XPS of E-MoS2/C electrode, it is reasonable that the E-MoS2/C underwent a conversion reaction during sodiation/desodiation.

As presented in Fig. 3b, the cyclic voltammograms (CV) show the electrochemical reactions in details, consistent with the potential plateaus observed in the charge/discharge curves. The CV profiles could be well repeated in following cycles, indicating that the high reversiblity of the conversion reaction. The cycling performances of P-MoS_2, E-MoS_2 and E-MoS_2/C were tested in the electrolyte with PC. As shown in Fig. S7, It is obvious that E-MoS_2/C shows the best electrochemical properties, mainly ascribed to the improved conductivity of the composite. More importantly, they are attributed to the fact that the thinner nanosheets are capable of shortening the Na-ion diffusion length as well.

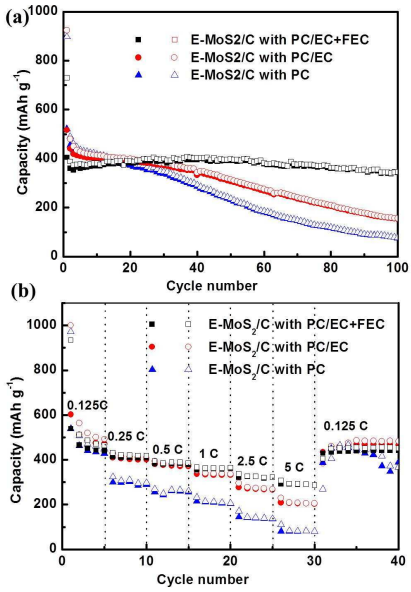

Fig. 4 (a) Cycling performances at 100 mA g^{-1}; (b) Rate capability of E-MoS_2/C in various electrolytes during 0.01-2.5 V.

In order to further improve the electrochemical properties of E-MoS_2/C, different electrolytes were utilized. As shown in Fig. 4a, the reversible capacities with PC and PC/EC are almost the same for the first 20 cycles with the value of ~400 mAh g^{-1}, but then decrease to 75.7 mAh g^{-1} and 152.8 mAh g^{-1}, respectively, after 100 cycles. Compared to PC, PC/EC solvent has higher conductivity and lower viscosity,[17] so that it can lead to higher capacity retention over longer cycling. Obvious capacity fades are observed for both PC and PC/EC after 30 cycles, which are ascribed to a kinetically limited process, such as electrolyte decomposition.[18] As reported previously, sodium anode would tend to be corroded continuously in the organic electrolytes, rather than allowing a stable SEI film to be formed.[19] In order to

Journal Name

Dynamic Article Links ►

Cite this: DOI: 10.1039/c0xx00000x

www.rsc.org/xxxxxx

ARTICLE TYPE

improve the performance of electrodes in SIBs, the film-forming additive, fluoroethylene carbonate (FEC), has recently been used to modify the SEI film of carbon anode [20] and Sb/C anode.[21] FEC has been bserved to form a passivation film at 0.7 V on both the carbon and the sodium surfaces, thereby protecting the electrodes from further side reactions with the solvents. A compact SEI film that is likely to be composed of stable alkali fluoride or fluroalkyl carbonate was inferred to be formed on the Sb/C. Therefore, E-MoS_2/C was further tested in the electrolyte with the addition of 5 wt % FEC. It could maintain an almost stable capacity of 390 $mAhg^{-1}$ over 100 cycles, which realized the 77.8 % of the theoretical capacity (668.0 mAh g^{-1}) based on conversion reactions. The significant improvement of cycling behavior resulted from the effect of the FEC additive, which could enhance the structural stability of the SEI film and thus curb further electrolyte decomposition. The rate capabilities of E-MoS_2/C with various electrolytes are evaluated in Fig. 4b. The electrodes deliver average capacities of 467.7 mAh g^{-1}, 509.6 mAh g^{-1}, and 460.7 mAh g^{-1} for PC/EC+FEC, PC/EC, and PC at 0.125 C, respectively. When the current rate increases gradually to 5 C, the capacities decrease to 290.1 mAh g^{-1}, 205.7 mAh g^{-1}, and 81.3 mAh g^{-1}, respectively. The capacity retention is presented in Fig. S8, which is 62.0 %, 40.3 %, and 17.6 % for PC/EC+FEC, PC/EC, and PC at 5C, respectively. The excellent rate capability with FEC additive is likely to be due to the higher ionic conductivity of the SEI film. From its first charge/discharge curve (Fig. S4d), we can only infer that a stable SEI film is probably formed within the range of 0.8-1.25 V. Further investigations of the components, the formation process, and the ionic conductivity for this SEI layer are needed in the future. We also tested the electrochemical performance of E-MoS_2/C at different cut-off voltages in Fig. S9, interestingly, the results demonstrate the cut-off voltages play a key role to determine the reaction mechanisam and provide a comprehensive reference for future researches.

In summary, we successfully applied MoS_2 with highly improved capacity through conversion reaction in a rechargeable sodium battery. Several strategies were exploited to progressively optimize its Na-storage properties, including the exfoliation of MoS_2 layers, the incorporation of carbon, and the optimization of the electrolyte system. As a result, E-MoS_2/C in 1.0 M $NaClO_4$ with PC/EC+FEC achieved a high reversible capacity and exhibited excellent rate capability. Our findings have therefore revealed a promising anode material candidate for a high-capacity and long-life sodium ion battery.

This work was financially supported by the Australian Research Council through a Discovery Project (DP110103909). The authors acknowledge use of the facilities at the UOW Electron Microscopy Centre funded by Australian Research Council grants (LE0882813and LE0237478). The authors would like to thank Dr Tania Silver for critical reading of the manuscript.

Notes and references

[a]*Institute for Superconducting & Electronic Materials (ISEM),Innovation Campus, University of Wollongong, Wollongong, NSW, 2519, Australia. Tel: +61-2-4298-1405; Fax: +61-2-4221-5731;E-mail:shulei@uow.edu.au*

† Electronic Supplementary Information (ESI) available: See DOI: 10.1039/b000000x/

1 J. M. Tarascon, M. Armand, *Nature* 2001, **414**, 359-367 .
2 J. B. Goodenough, Y. Kim, *Chem. Mater.* 2010, **22** , 587-603.
3 X. Wang, Q. Qu, Y. Hou, F.Wang, Y. Wu, *Chem Commu.,* 2013, **49**, 6179-6181.
4 B. Zhang, Y. Liu, X. Wu, Y. Yang, Z. Chang, Z. Wen, Y. Wu, *Chem Commu.,* 2014, **50**, 1209-1211.
5 H. Zhang, X. Wu, T. Yang, S. Liang, X. Yang, *Chem Commu.,* 2013, **49**, 9977-9979.
6 S.-W. Kim, S.-H. Seo, X.Hua, G. Ceder, K. Kang, *Adv. Energy Mater.* 2012, **2**, 710-721.
7 A. B. Laursen, S. Kegnaes, S. Dahl, I Chorkendorff, *Energy Environ. Sci.* 2012, **5**, 5577-5591.
8 R. Tenne, *Nature Nanotech.* 2006, **1**, 103-111.
9 Z. Lu, A. Schechter, M. Moshkovich, D. Aurbach, *J. Electroanal. Chem.* 1999, **466,** 203-217.
10 Y. Liang, R. Feng, S. Yang, H. Ma, J. Liang, J. Chen. *Adv. Mater.* 2011, **23**, 640-643.
11 K. Chang, W. Chen. *Chem. Comm.,* 2011, **47**, 4254-4254.
12 S. Ding, D. Zhang, J. S. Chen, X. W. Lou, *Nanoscale* 2012, **4**, 95-98.
13 H. Liu, D. Su, R. Zhu, B. Sun, G. Wang, S. Z. Qiao, *Adv. Energy Mater.* 2012, **2**, 970-975.
14 J. Park, J.-S. Kim, J.-W. Park, T.-H. Nam, K.-W. Kim, J.-H. Ahn, G. Wang, H.-J. Ahn. *Electrochimi. Acta.* 2013, **92**, 427-432.
15 Y.-X. Wang, S.-L. Chou, D. Wexler, H.-K. Liu, S.-X. Dou, *Chemistry-A European Journal,* 2014, DOI: 10.1002/chem.201402563R1.
16 K. Chang, W. Chen, L. Ma, H. Li, H. Li, F. Huang, Z. Xu, Q. Zhang, J.-Y. Lee, *J. Mater. Chem.* 2011, **21**, 6251-6257.
17 A. Ponrouch, E. Marchante, M. Courty, J.-M. Tarascon, M. R. Palacin, *Energy Environ. Sci.* 2012, **5**, 8572-8583.
18 A. Ponrouch, P. L. Taberna, P. Simon, M. R. Palacín, *Electrochim. Acta.* 2012, **61**, 13-18.
19 M. D. Slater, D. Kim, E. Lee, C. S. Johnson, *Adv. Funct. Mater.* 2012, DOI: 10.1002/adfm.201200691.
20 S. Komaba , T. Ishikawa , N. Yabuuchi , W. Murata, A. Ito , Y. Ohsawa, *ACS Appl. Mater. Interfaces* 2011, **3**, 4165-4168.
21 J. Qian, Y. Chen, L, Wu, Y. Cao, X. Ai, H. Yang, *Chem. Commun.* 2012, **48**, 7070-7072.

Journal Name

Dynamic Article Links ►

Cite this: DOI: 10.1039/c0xx00000x

www.rsc.org/xxxxxx

ARTICLE TYPE

TOC

Reversible Sodium Storage by Conversion Reaction in MoS_2/C Composite

Yun-Xiao Wang,[a] Kuok Hau Seng,[a] Shu-Lei Chou,*[a] Jiazhao Wang,[a] Zaiping Guo,[a] David Wexler,[a] Hua-Kun Liu,[a] Shi-Xue Dou[a]

Keywords: exfoliated MoS_2, anode, sodium-ion battery, Na-storage mechanism, FEC additive.

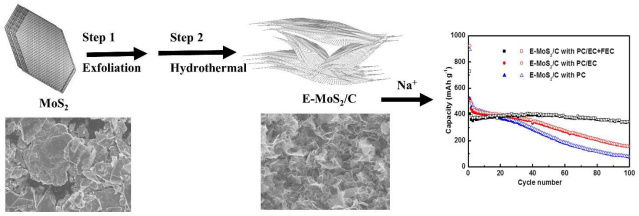

Exifoliated MoS_2/C composite serves as a novel anode material for the sodium ion battery for the first time, exhibiting high capacity and prolonged cycling life. The unique structure and optimized electrolyte effectively promote Na-storage performance. This work suggests a promising new anode and paves the way to further explore its great potential for large-scale applications.

Journal Name

Dynamic Article Links ►

Cite this: DOI: 10.1039/c0xx00000x

www.rsc.org/xxxxxx

ARTICLE TYPE

Supporting information

Reversible Sodium Storage by Conversion Reaction in MoS_2/C Composite

Yun-Xiao Wang,[a] Kuok Hau Seng,[a] Shu-Lei Chou,*[a] Jiazhao Wang,[a] Zaiping Guo,[a] David Wexler,[a] Hua-Kun Liu,[a] Shi-Xue Dou[a]

Journal Name

Dynamic Article Links ►

Cite this: DOI: 10.1039/c0xx00000x

www.rsc.org/xxxxxx

ARTICLE TYPE

Experimental

Material synthesis

Synthesis of exfoliated MoS_2/C composite: Firstly, exfoliated MoS_2 (E-MoS_2) was prepared from pristine MoS_2 (P-MoS_2) via a modified exfoliation method in a previous report.[21] Exfoliated MoS_2/C composite (E-MoS_2/C) was fabricated by the hydrothermal method in the second step. Specifically, 0.27 g glucose was dissolved in 20 mL deionized water, then mixed with 40 mL E-MoS_2 dispersion (4.2 mg mL^{-1}). The obtained mixture was loaded into a Teflon-lined autoclave, which was then sealed and maintained at 150 ^{o}C for 5 h, and then allowed to cool down to room temperature naturally. After centrifugation, the black product was then washed three times each with deionized water and absolute ethanol, and dried under vacuum at 80 ^{o}C overnight. The E-MoS_2/C was finally obtained after annealing treatment at 450 ^{o}C for 2 h and then at 800 ^{o}C for 2 h in a mixed 5 % H_2/Ar atmosphere.

Structural characterization

The morphologies of the samples were investigated by field-emission scanning electron microscopy (FESEM; JEOL JSM-7500FA) and transmission electron microscopy (TEM, JEOL 2011, 200 keV). The XRD patterns were collected by

Journal Name

Dynamic Article Links ►

Cite this: DOI: 10.1039/c0xx00000x

www.rsc.org/xxxxxx

ARTICLE TYPE

powder X-ray diffraction (XRD; GBC MMA diffractometer) with Cu Kα radiation at a scan rate of 1° min^{-1}. Thermogravimetric analysis (TGA) was performed in air with a SETARAM Thermogravimetric Analyzer (France). Ex-situ XPS and XRD were taken on the electrodes at different charging or discharging states. The ex-situ XRD samples were prepared by peeling the electrode materials off the Cu current collector, and using Kapton tape to seal onto XRD holder inside of a glove box. This process can avoid the disturbance of strong Cu peaks and the oxidation of electrode material. The X-ray photoelectron spectra (XPS) experiment was carried out using Al Kalpha radiation and fixed analyser transmission mode. The pass energy was 60 eV for the survey spectra and 20 eV for specific elements. The XPS samples were stored in argon box before test.

Electrochemical measurements

The electrochemical measurements were conducted by assembling coin-type half cells in an argon-filled glove box. The slurry was prepared by fully mixing 80 wt % active materials (P-MoS_2, E-MoS_2, and E-MoS_2/C), 10 wt % carbon black, and 10 wt % polyvinylidene difluoride (PVdF) by planetary mixer (KK-250S). Then, the obtained slurry was pasted on a copper film using a doctor blade with a thickness of 100 μm, which was followed by drying in a vacuum oven overnight at 80 °C. The working electrode was prepared by punching the electrode film into discs 0.97 cm in diameter.

Journal Name

Dynamic Article Links ►

Cite this: DOI: 10.1039/c0xx00000x

www.rsc.org/xxxxxx

ARTICLE TYPE

The sodium foil was cut using a surgical blade from sodium bulk stored in mineral oil. The sodium foil was employed as both reference and counter electrode. The electrodes were separated by a glass fiber separator. Several electrodes with various electrolytes were tested in our work, including P-MoS_2 in 1.0 M $NaClO_4$ with PC (P-MoS_2 with PC), E-MoS_2 in 1.0 M $NaClO_4$ with PC (E-MoS_2 with PC), exfoliated MoS_2/C in 1.0 M $NaClO_4$ with PC (E-MoS2/C with PC), E-MoS_2/C in 1.0 M $NaClO_4$ with PC/EC (E-MoS_2/C with PC/EC), and exfoliated MoS_2/C in 1.0 M $NaClO_4$ with PC/EC + 5 wt % FEC (E-MoS_2/C with PC/EC+FEC). The electrochemical performances were tested on a LAND Battery Tester. Cyclic voltammetry was performed using a Biologic VMP-3 electrochemical workstation.

Journal Name

Dynamic Article Links ►

Cite this: DOI: 10.1039/c0xx00000x

www.rsc.org/xxxxxx

ARTICLE TYPE

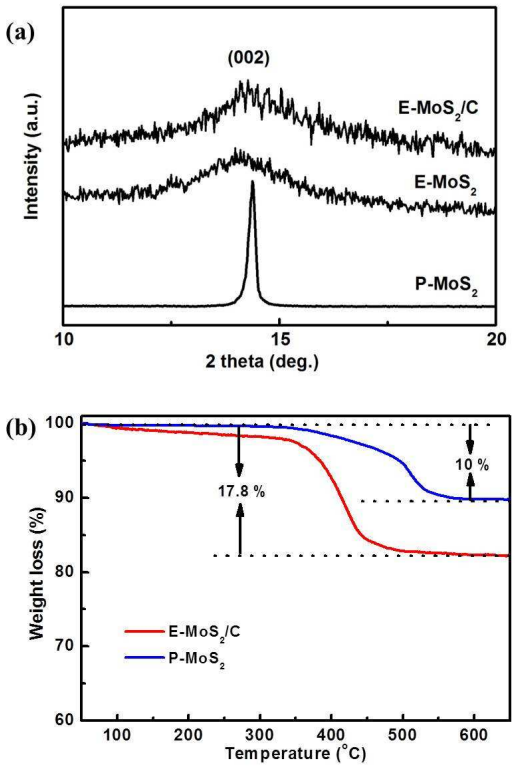

Fig. S1. XRD patterns at range of 10^{o} - 20^{o} P-MoS_2, E-MoS_2, and E-MoS_2/C. (a) TGA curves of P-MoS_2 and E-MoS_2/C.

The TGA curve of P-MoS_2 is used as a reference, showing a 10 % weight loss after heating to 650 ^{o}C in air atmosphere, which indicates that the remaining product after the TGA measurement is pure MoO_3. Based on this fact and assuming that the amorphous carbon is completely decomposed after 650 ^{o}C, it is estimated that the

Journal Name

Dynamic Article Links ►

Cite this: DOI: 10.1039/c0xx00000x

www.rsc.org/xxxxxx

ARTICLE TYPE

MoS_2 content in the composite is approximately 91 wt%, with successful incorporation of about 9 wt% carbon in the E-MoS_2/C.

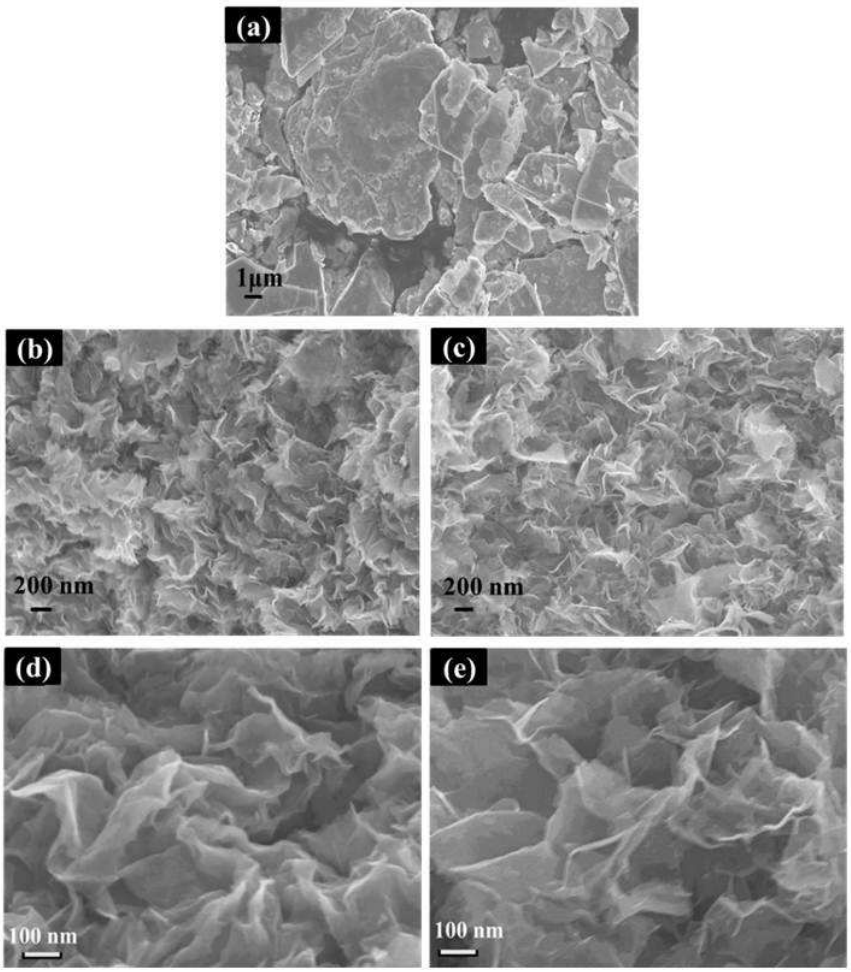

Fig. S2. SEM images of (a) P-MoS_2, (b) E-MoS_2 and (c) E-MoS_2/C at low magnification. SEM images of (d) E-MoS_2 and (e) E-MoS_2/C at high magnification.

Journal Name

Dynamic Article Links ►

Cite this: DOI: 10.1039/c0xx00000x

www.rsc.org/xxxxxx

ARTICLE TYPE

Morphological investigations of P-MoS_2, E-MoS_2, and E-MoS_2/C are shown by the SEM images in Fig. S2a-e. Unlike the P-MoS_2 bulk, E-MoS_2 and E-MoS_2/C are in the form of crumpled sheets. This demonstrates the successful exfoliation of the P-MoS_2 into graphene-like nanosheets. Furthermore, it is notable that the nanosheets of E-MoS_2/C are thinner than those of E-MoS_2, indicating that the E-MoS_2/C nanosheets are composed of fewer MoS_2 layers and that the incorporation of carbon restrains the restacking of the MoS_2 layers. This can be further confirmed by SEM images at higher magnification.

Journal Name

Dynamic Article Links ►

Cite this: DOI: 10.1039/c0xx00000x

www.rsc.org/xxxxxx

ARTICLE TYPE

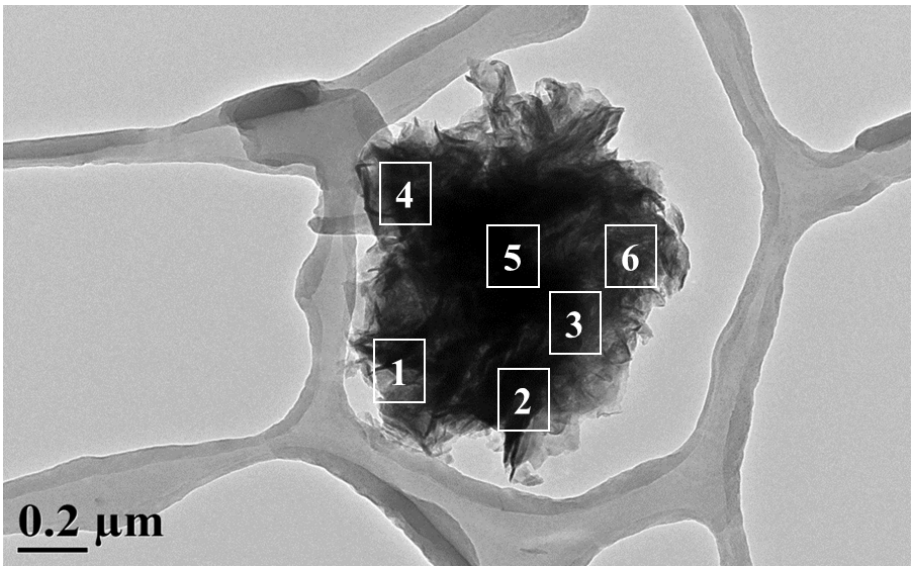

1 Element	Mass%	Atom%	2 Element	Mass%	Atom%
C K	17.42	55.67	C K	15.00	60.39
S K	12.22	14.62	S K	10.08	15.21
Cu K	7.62	4.60	Cu K	5.27	4.01
Mo L *	62.74	25.10	Mo L *	69.66	20.39
3 Element	Mass%	Atom%	**4** Element	Mass%	Atom%
C K	19.91	58.83	C K	43.53	81.97
S K	13.73	15.19	S K	8.38	5.91
Cu K	7.63	4.60	Cu K	6.43	2.29
Mo L *	58.72	21.72	Mo L *	41.66	9.82
5 Element	Mass%	Atom%	**6** Element	Mass%	Atom%
C K	17.66	55.01	C K	22.40	61.41
S K	15.09	17.60	S K	15.59	16.01
Cu K	5.86	3.45	Cu K	7.42	3.84
Mo L *	61.38	23.93	Mo L *	54.59	18.74

Journal Name

Dynamic Article Links ►

Cite this: DOI: 10.1039/c0xx00000x

www.rsc.org/xxxxxx

ARTICLE TYPE

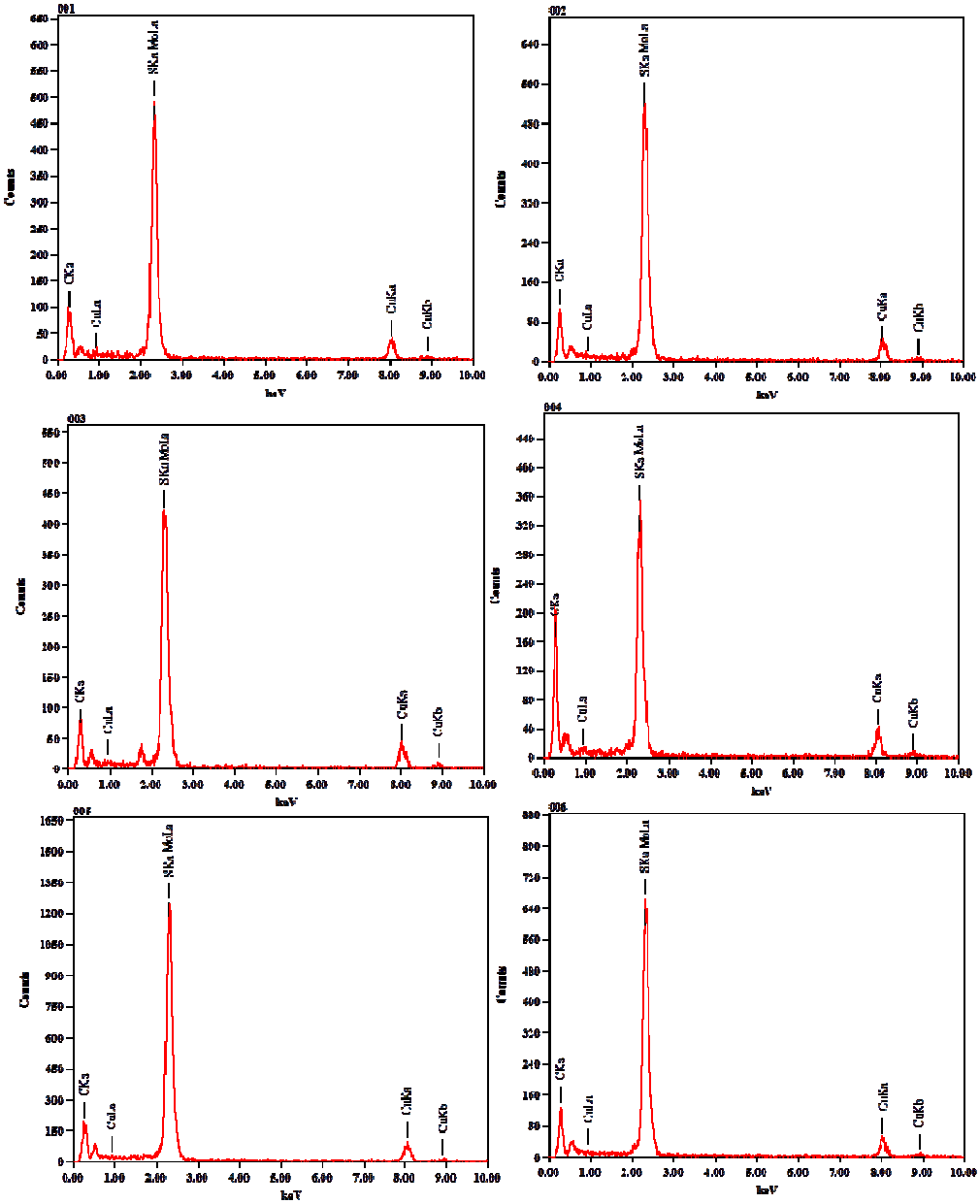

Fig. S3. EDX analysis of E-MoS_2/C flake with six spots.

Journal Name

Dynamic Article Links ►

Cite this: DOI: 10.1039/c0xx00000x

www.rsc.org/xxxxxx

ARTICLE TYPE

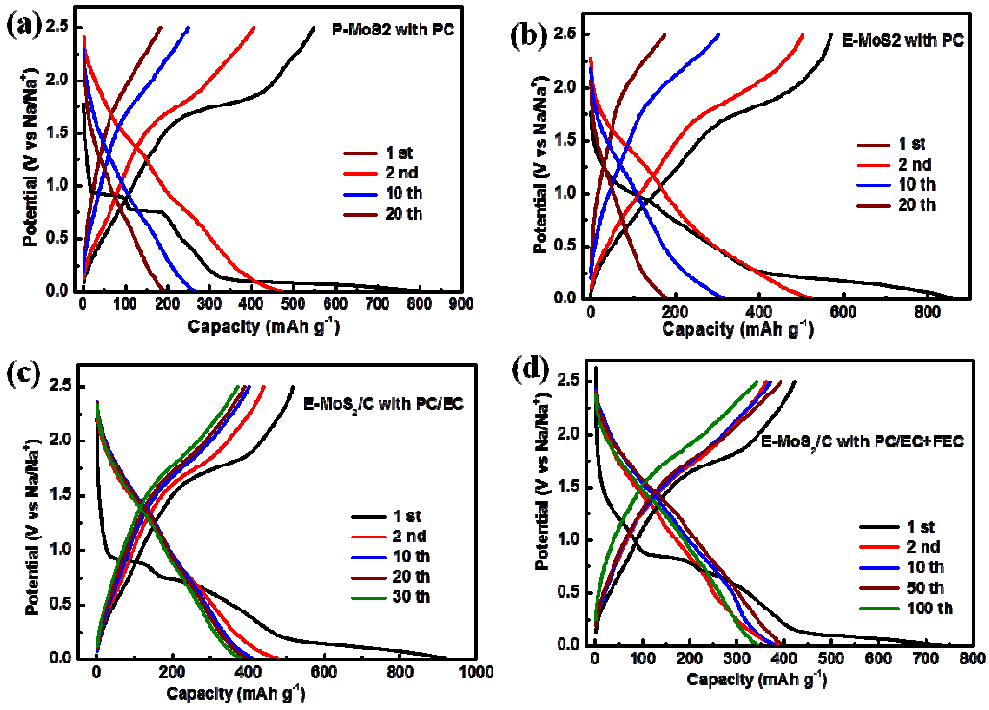

Fig. S4. Charge/discharge profiles of (a) P-MoS_2 with PC, (b) E-MoS_2 with PC, (c) E-MoS_2/C with PC/EC and (d) E-MoS_2/C with PC/EC+FEC. All the electrodes were tested at a current density of 100 mA g^{-1}.

Journal Name

Dynamic Article Links ►

Cite this: DOI: 10.1039/c0xx00000x

www.rsc.org/xxxxxx

ARTICLE TYPE

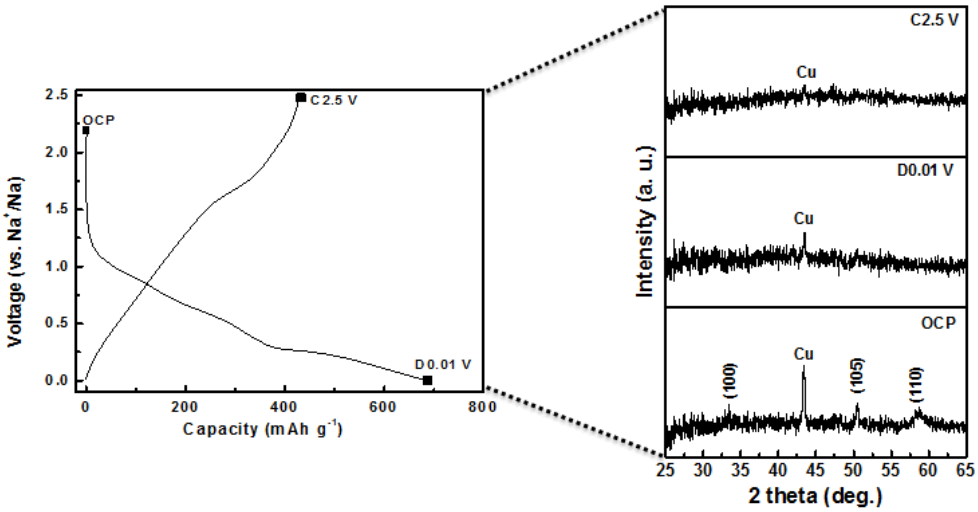

Fig. S5 (a) Initial charge/discharge curves at current rate of 10 mA g^{-1} and (b) corresponding ex-situ XRD patterns for different states of E-MoS_2/C in 1.0 M $NaClO_4$ with PC: OCP (open circuit potential), D0.01 V(discharged to 0.01 V) and C2.5 V (charged back to 2.5 V).

The XRD patterns shown in Fig. S5b were subtracted the background of Kapton tape. The fresh electrode coated by Kapton tape can show three typical peaks of E-MoS_2/C, which were indexed to (100), (105), and (110). A small peak located at ~43.5 ^{o} was attributed to the Cu from the current collector. When the electrode was fully discharged to 0.01 V, all of diffraction peaks disappeared and the electrode material showed the amorphous nature. It maintained amorphous when the electrode material

Journal Name

Dynamic Article Links ►

Cite this: DOI: 10.1039/c0xx00000x

www.rsc.org/xxxxxx

ARTICLE TYPE

was fully charge back to 2.5 V. The results indicate that E-MoS_2/C may undergo a conversion reaction during the charge/discharge process.

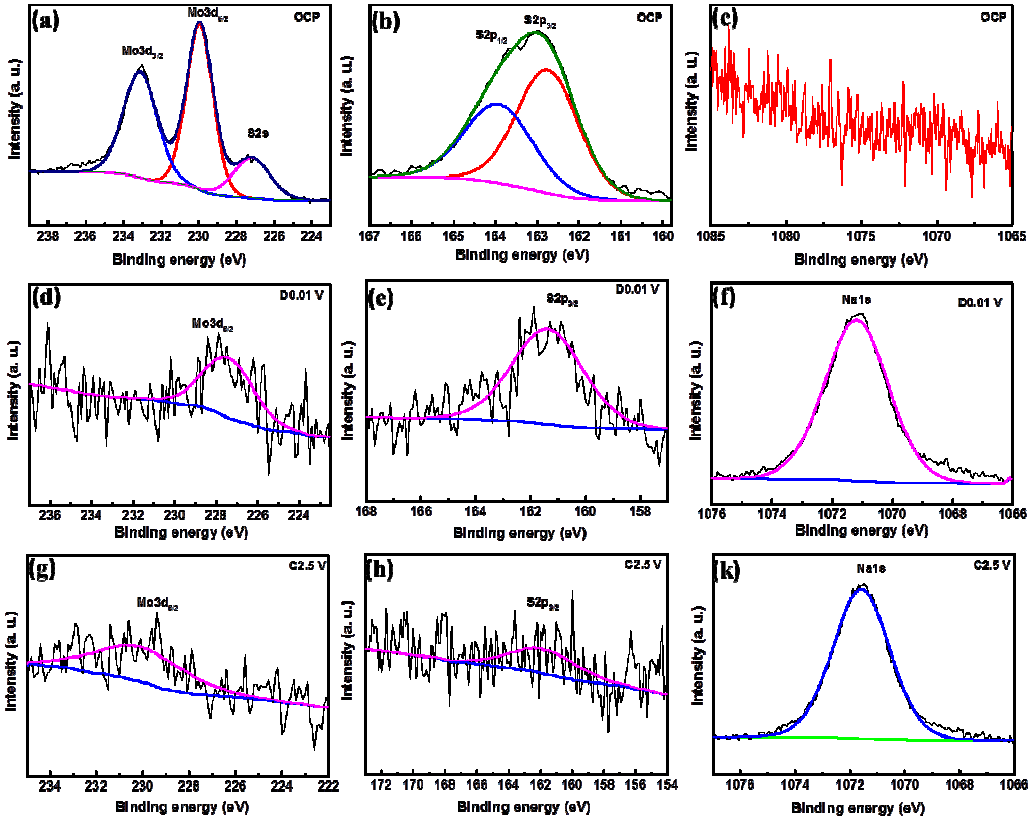

Fig. S6 The XPS spectrum for different states of E-MoS_2/C in 1.0 M $NaClO_4$ with PC: (a), (d), and (g) Mo 3d spectrum at OCP, D0.01 V, and C2.5 V; (b), (e), and (h) S 2p spectrum at OCP, D0.01 V, and C2.5 V; (c), (f), and (k) Na 1s at OCP, D0.01 V, and

Journal Name

Dynamic Article Links ►

Cite this: DOI: 10.1039/c0xx00000x

www.rsc.org/xxxxxx

ARTICLE TYPE

C2.5 V.

Further evidence for MoS_2-Na conversion reaction was provided from XPS analysis. For the E-MoS_2/C electrode at OCP state, the Fig. S6a shows the predominant peaks at ca. 229.7 and 232.8 eV, which is ascribed to $Mo3d_{5/2}$ and $Mo3d_{3/2}$ binding energies, respectively. Correspondingly, the peaks at ca. 162.5 and 163.4 eV can be attributed to $S2p_{3/2}$ and $S2p_{1/2}$ binding energies, respectively. The well-defined spin-coupled Mo and S doublets demonstrate the hexagonal MoS_2 state. No sodium element is observed for the fresh electrode. When the electrode was charged to 0.01 V, the $Mo3d_{5/2}$ peak (Fig. S6a) shifts to ca. 227.5 eV, indicating the reduction of Mo^{4+} to Mo. A distinguished peak at ca.1071.2 eV in Fig. S6c can be indexed to the Na1s. The $S2p_{3/2}$ peak shifts to 161.5 eV, which indicates the presence of Na_2S. When it was charged to 2.5 V, the $Mo3d_{5/2}$ peak appears at higher binding energy (~230.4 eV), and the S1s energy binding is ~162.1 eV. This indicates the recovery of MoS_2. The Na1s peak at ca. 1071.5 eV is probably ascribed to Na_2CO_3 in solid electrolyte interphase (SEI) film. It is noticeable that the intensity of $Mo3d_{5/2}$ and S1s for MoS_2 is severely lowered, which is likely due to that the formation of thick SEI film on electrode surface. Combining the ex-situ XRD and XPS of E-MoS_2/C electrode, it is reasonable that the E-MoS_2/C underwent a conversion reaction during sodiation/desodiation.

Journal Name

Dynamic Article Links ►

Cite this: DOI: 10.1039/c0xx00000x

www.rsc.org/xxxxxx

ARTICLE TYPE

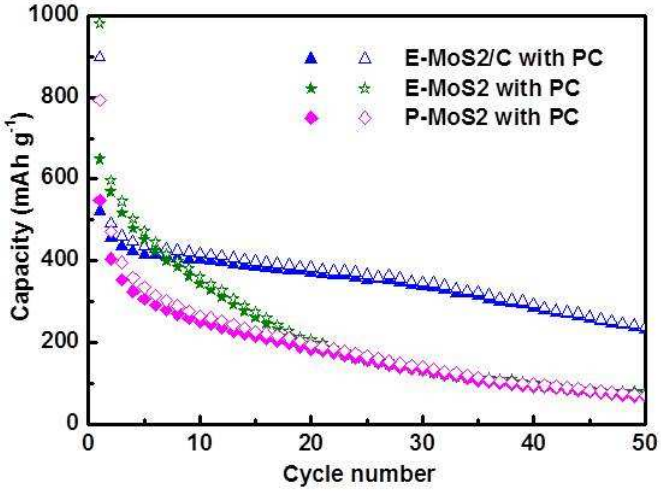

Fig.S7 Cycling performances of E-MoS_2/C in various electrolytes. The applied current density was 100 mA g^{-1} at 0.01-2.5 V for all electrodes. The solid and open symbols represent charge and discharge capacities, respectively.

Both P-MoS_2 and E-MoS_2 show similar cycling performance after 20 cycles. E-MoS_2 shows higher capacity than P-MoS_2, with average reversible capacity of 366.2 mAh g^{-1} and 275.3 mAh g^{-1} in the initial 20 cycles, respectively. This indicates that the E-MoS_2 can accommodate more Na ions due to the d-spacing enlargement effect, while it shows almost the same electrochemical performance as P-MoS_2 for prolonged

Journal Name

Dynamic Article Links ►

Cite this: DOI: 10.1039/c0xx00000x

www.rsc.org/xxxxxx

ARTICLE TYPE

cycling as a result of its severe restacking. For E-MoS_2/C, the incorporation of carbon can significantly improve the capacity retention.

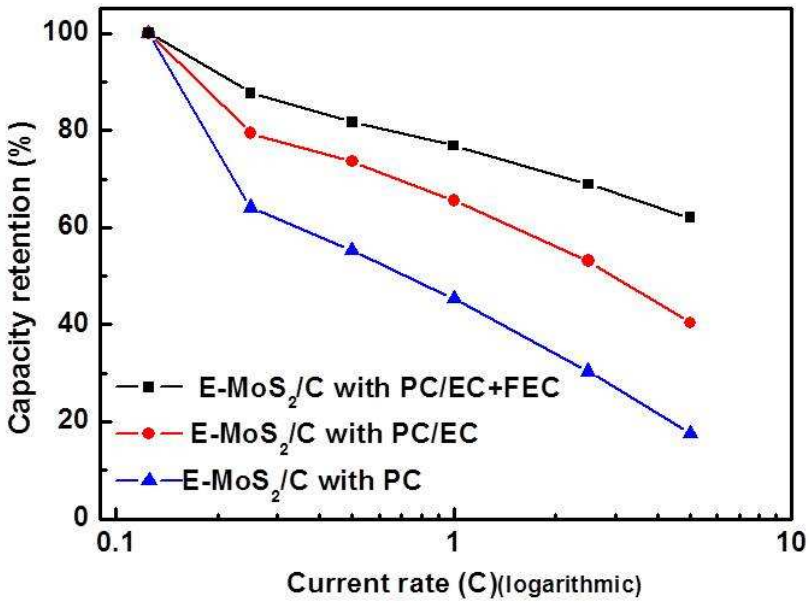

Fig.S8 Capacity retention of E-MoS_2/C in various electrolytes at different current densities.

Journal Name

Dynamic Article Links ►

Cite this: DOI: 10.1039/c0xx00000x

www.rsc.org/xxxxxx

ARTICLE TYPE

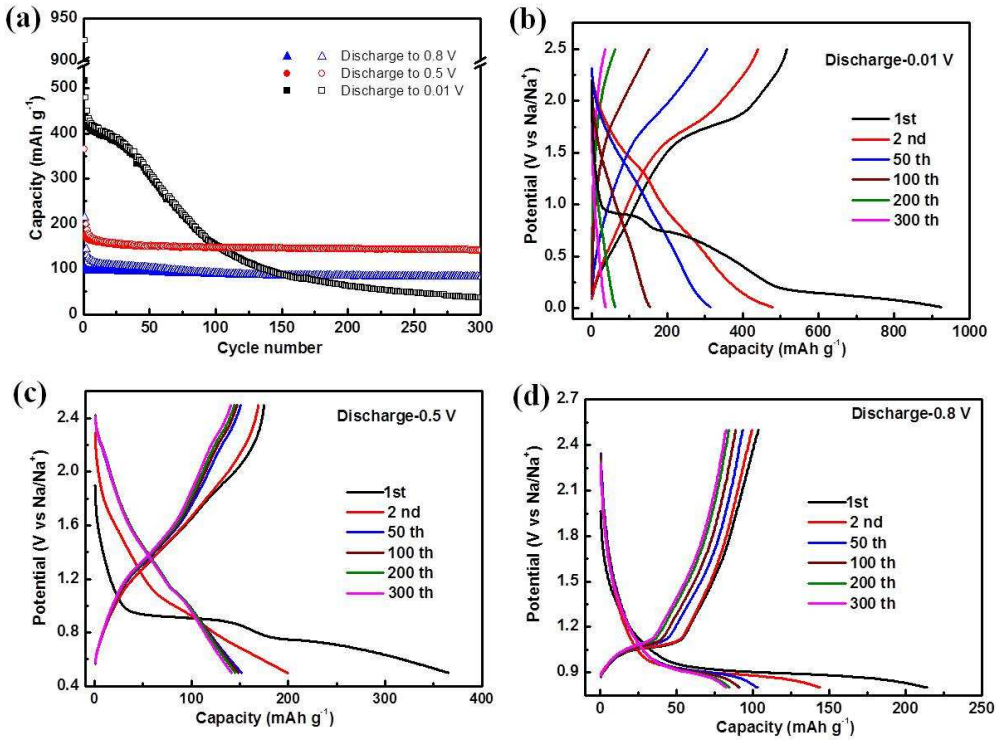

Fig. S9. Cycling performances (a) and charge/discharge profiles (b) of E-MoS_2/C in the voltage ranges from 2.5 V to 0.8 V, 0.5 V, and 0.01 V in 1.0 M NaClO4 with PC.

It is worth noting that the E-MoS_2/C in 1 M $NaClO_4$ with PC exhibited distinct cycling performances for different discharge cut-off voltages. In the range of 0.01-2.5 V, the electrode delivers the highest average capacity of 375.5 mAh g^{-1} for the initial 50 cycles, while it shows serious capacity degradation in successive cycles. When the discharge voltages are cut off at 0.8 V and 0.5 V, even though the capacities decrease to ~83 mAh g^{-1} and ~140 mAh g^{-1}, respectively, no capacity decay is observed over 300 cycles.

Journal Name

Dynamic Article Links ►

Cite this: DOI: 10.1039/c0xx00000x

www.rsc.org/xxxxxx

ARTICLE TYPE

When MoS_2/C composite electrode was tested between 2.5 and 0.8 V (Fig. S9d), the charge/discharge curves show repeatable plateau for 300 cycles, which confirmed the intercalation/deintercalation process with no change of MoS_2 layer structure. When discharge to 0.5 V, it also showed good cycling stability, which is consistent with the intercalation/deintercalation process with distortion of MoS_2 layer structure. The charge/discharge curves are slope curves instead of obvious plateaus. However, when it was fully discharged to 0.01 V, the distorted MoS_2 was further react with Na ions, which is corresponding to the conversion reaction. This process leads to higher capacity and the conversion reaction process for the following cycles.